Eur. Phys. J. D **34**, 29–34 (2005)
DOI: 10.1140/epjd/e2005-00112-y

THE EUROPEAN PHYSICAL JOURNAL D

Structure of unsupported antimony nanoclusters

M. Kaufmann[1,2], A. Wurl[1,2], J.G. Partridge[1,2], and S.A. Brown[1,2,a]

[1] Nanostructure Engineering Science and Technology (NEST) Group and the MacDiarmid Institute of Advanced Materials and Nanotechnology, University of Canterbury, New Zealand
[2] Department of Physics and Astronomy, University of Canterbury, Private Bag 4800, New Zealand

Received 6 September 2004
Published online 13 July 2005 –

Abstract. In this study we present results of electron diffraction experiments on unsupported antimony nanoclusters with mean sizes in the range of 20–40 nm. An inert-gas aggregation source was used to produce the cluster beam. Electron diffraction patterns reveal phase transitions between crystalline and amorphous phases as well as particles composed of Sb_4 tetramers. The diffraction results are correlated with electron microscope investigations of the morphology of films formed by deposition of the clusters.

PACS. 36.40.-c Atomic and molecular clusters – 61.46.+w Nanoscale materials: clusters, nanoparticles, nanotubes, and nanocrystals – 61.14.-x Electron diffraction and scattering

1 Introduction

Bulk antimony has two known allotropes: the 'grey' metallic form with a rhombohedral structure and the 'black' amorphous form [1]. While phosphorus and arsenic have a solid modification consisting of tetramers ('white' phosphorus and 'yellow' arsenic), there has been no such structure observed for Sb, apart from a report of crystalline order in Sb thin films [2].

Sattler et al. were the first to study Sb clusters extensively [3]. Using mass spectrometry techniques they showed that Sb vapour consists mainly of tetramers. If the vapour is supersaturated in cold inert gas, these Sb_4 particles condense to form larger clusters with magic numbers. To explain these magic numbers Sattler proposed a model for the packing of Sb_4 tetrahedra which, in fact, results in clusters with an fcc structure. This unusual and interesting phase has, however, not been observed directly.

While electron diffraction has been used for a long time to analyse the structure of bulk materials, it is also an excellent tool for analysing the structure of nanoclusters. Diffraction of unsupported particles in a molecular beam is particularly advantageous as there is no interaction between particles and substrate. Additionally, the time the clusters are exposed to the electron beam is very short minimising the influences of the beam. Hence electron diffraction allows the study of the unperturbed, intrinsic structures of nanoparticles.

Stein et al. studied the structure of unsupported Sb clusters using electron diffraction [4]. When using argon as cooling gas, a rhombohedral structure was observed, as in bulk Sb, however, the diffraction patterns were too weak to draw further conclusions. Using a different cluster source which did not use a cooling gas, Stein observed an amorphous structure. In a similar study Sun et al. observed liquid clusters when using helium as cooling gas [5].

There is still no comprehensive knowledge of the structure of unsupported Sb clusters. In the context of the known allotropes of bulk Sb, possible structures and phase transitions of Sb clusters are of considerable interest. This paper presents evidence for structural phase transitions in Sb clusters and discusses the observations in relation to the known bulk structures.

2 Experimental procedure

In our experiment a molecular beam of Sb clusters is produced in an inert-gas aggregation source using Ar and He as cooling gases. The mixture of clusters and gas is extracted through a series of nozzles by two differential pumping stages, thereby removing the carrier gas and forming a cluster beam. This cluster beam is then probed by an 80 kV electron beam. The electrons are scattered by the randomly oriented clusters resulting in a Debye-Scherrer powder diffraction pattern which is detected by a pair of linear diode array (LDA) chips aligned along the diameter of the ring pattern. This equipment has been used previously to study the structure of Cu, Ag, Pb, and Bi clusters [6–10].

Several parameters have been used to control the structure of the particles in the beam: the temperature of the crucible T_C, the type of cooling gas (Ar or He) and the source inlet gas flow rate (and thereby the inert-gas

[a] e-mail: simon.brown@canterbury.ac.nz

pressure in the source P_G which increases with increasing flow rate). Additionally, the geometry of the nozzles can be adjusted.

During some of the diffraction experiments, clusters were deposited on SiO_2 and SiN substrates. These samples were then studied in a Field-Emission Scanning Electron Microscope (FE-SEM) to obtain information about the size distribution of the clusters in the beam and the morphology of the resulting cluster films. The mean size is determined by measuring the diameter of clearly defined particles on the substrate and the uncertainty is given as the standard deviation of the particle size distribution. It is, however, important to consider the possibility that the clusters change their shape and size through interaction with the substrate or diffusion. Diffusion is very unlikely due to the rms roughness ($\sim$10 nm) of the silicon dioxide samples used here. Studies of bouncing Sb clusters of similar sizes in the same apparatus [11] lead us to believe that deformation and/or fragmentation due to cluster-surface interaction are not relevant.

Before the analysis of the experimental patterns, the diffraction signal due to the gas background (measured immediately before or after each run) is subtracted from the raw data. In order to determine the structure of the clusters the background-subtracted data is compared to calculated diffraction patterns. The calculations are based on the kinematical diffraction theory, in particular the Debye formula [12]. The structures used for the calculations were the rhombohedral bulk structure of Sb [13], the structure of Sb_4 tetramers [14,15], and the structure of liquid Sb [16]. The fcc structures proposed by Sattler [3] were clearly not relevant to the experimental diffraction patterns obtained here [17].

3 Results and analysis

3.1 Experiments using argon as cooling gas

During the diffraction experiments in which Ar was used as the source cooling gas, cluster production was controlled using two parameters: the crucible temperature T_C and the gas flow rate. The temperature range used for these experiments was 600−800 °C and the range of Ar flow rates was 50–200 sccm.

Figure 1a shows that at low Ar flow rate ($\leq$100 sccm) broad peaks are observed at $s \sim 0.33\,(1/\text{Å})$ and at $s \sim 0.52\,(1/\text{Å})$. Increasing the gas flow rate leads to a split in the second peak while the first peak gets narrower (Fig. 1b). When the flow rate is further increased the peaks become narrower again and new peaks appear at higher s-values (Fig. 1c), resulting in patterns which are consistent with calculated diffraction patterns for clusters with the symmetry of bulk rhombohedral Sb (dotted lines in Figs. 1c and 1f). Changing the source temperature leads to a similar result: at low temperature (<700 °C) the peaks are broad (Fig. 1d), while increasing the temperature leads to the bulk rhombohedral structure (Figs. 1e and 1f).

The peak positions in the diffraction patterns in Figures 1a and 1d agree well with the values found in the literature for amorphous Sb thin films [18,19] (note that the position of the second peak ($\sim$0.52 (1/Å)) in these patterns is clearly inconsistent with the patterns in Figs. 1c and 1f). As can be seen by the dotted line in Figure 1a the experimental patterns do not agree with the calculated pattern of a liquid Sb droplet [16] and so it is clear that the particles giving rise to the diffraction patterns in Figures 1a and 1d are amorphous.

The average size of the crystalline clusters has been estimated from the diffraction patterns (Figs. 1c and 1f) in two different ways. Firstly, the width of the first diffraction peak can be used to calculate the particle size from the Scherrer equation [12]. Secondly, the experimental diffraction patterns can be compared to calculated patterns from particles with a known size and structure. In Figure 1c the cluster size was estimated to be $\sim$3 nm using the Scherrer equation and $\sim$3.5 nm when comparing with model clusters. For Figure 1f the size estimates were $\sim$4.5 nm for both methods. The uncertainty for these values is $\pm$0.5 nm. The particle sizes obtained from FE-SEM images are discussed in Section 3.3.

3.2 Experiments using helium and a helium/argon mixture as cooling gas

The second set of experiments was carried out using helium and a helium/argon mixture (up to 20% Ar content) as the source cooling gas. The range of source temperatures used for these measurements was identical to that used in Section 3.1. The range of gas flow rates (300−1500 sccm), however, had to be significantly greater than for Ar in order to reach sufficiently high cluster beam intensities.

At low He flow rate (<800 sccm) and at all temperatures in the range 600–800 °C the diffraction patterns (Fig. 2a) show a single broad main peak at $s \sim 0.40\,(1/\text{Å})$ which is clearly broader and at a higher s-value than the main peak in Figure 1a. Increasing the He flow rate leads to a split in the first peak (Fig. 2b), and when the flow rate is further increased, peaks that are consistent with rhombohedral clusters are observed (Fig. 2c). Adding Ar to the He cooling gas leads to a similar result: at a low Ar content (<10%) there is a single broad main peak (Fig. 2d) and increasing the Ar content leads to the appearance of rhombohedral structure (Figs. 2e and 2f). Because of the high He flow rate used for the experiment shown in Figure 2f, these conditions are transient and very quickly lead to blocking of the nozzles. It was therefore not possible to deposit clusters in these conditions. The dotted lines in Figures 2a and 2d show the calculated diffraction pattern for Sb_4 tetramers which is in good agreement with the experimental data.

The mean size of the crystalline particles was estimated to be $\sim$3 nm for Figure 2c using the Scherrer equation and $\sim$3.5 nm for the comparison with calculated patterns. For Figure 2f both methods yield a mean size of $\sim$5 nm. The uncertainty for these values is $\pm$0.5 nm.

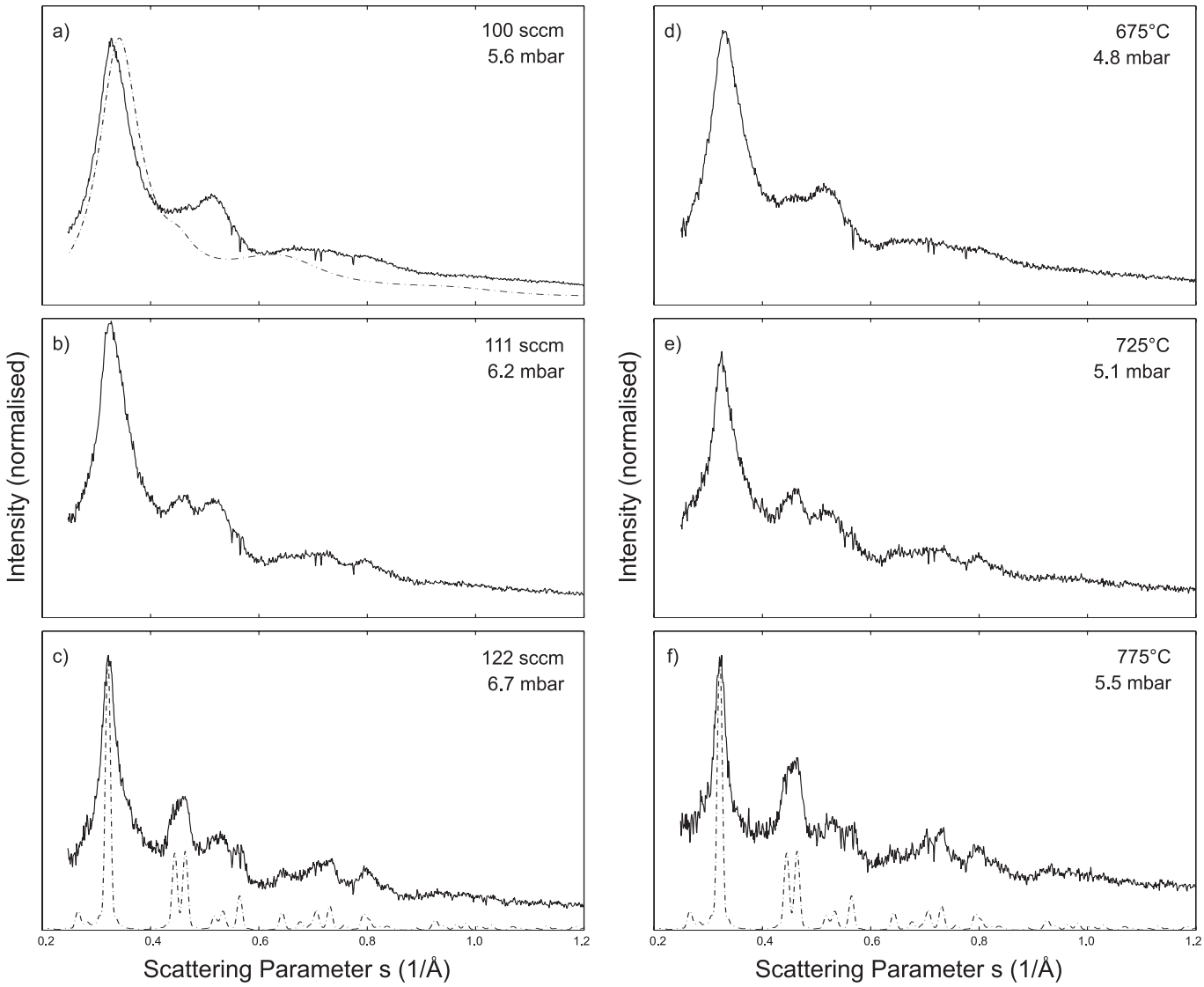

Fig. 1. Diffraction patterns of Sb clusters using Ar as cooling gas. (a–c) The gas flow rate is increased while leaving the temperature constant at 675 °C. (d–f) The temperature is increased while the gas flow rate is left constant at 82 sccm. The dotted line in figure (a) is the calculated pattern of a liquid Sb droplet and the dotted lines in figures (c) and (f) show the calculated pattern of a spherical particle with rhombohedral structure and 10 nm diameter. Note: there is no additional offset applied to any of the patterns but the calculated patterns are scaled to match the height of the experimental patterns. The background visible in the experimental patterns in (c) and (f) might be due to Sb tetramers.

The particle sizes obtained from FE-SEM images are discussed in Section 3.3.

3.3 FE-SEM studies of deposited clusters

To study the clusters under an FE-SEM they are deposited on Si wafers coated with either an oxide or nitride layer.

The amorphous clusters formed at low temperatures and low Ar flow rates (corresponding to the diffraction pattern in Fig. 1d) are shown in Figure 3. These clusters are spherical and have a narrow size distribution with a mean size of 40 ± 10 nm. The majority of these clusters bounce off the substrate's surface [11]. Clumps of clusters such as those shown in Figure 3 most likely arise due to the fact that they only stick to the surface when they hit a cluster or surface defect.

Figure 4a shows crystalline clusters corresponding to the diffraction pattern in Figure 2f while Figure 4b shows strongly facetted clusters produced at higher Ar flow rate and higher temperature. The crystalline particles are irregular in shape and have sizes ranging from 10 to over 100 nm. In Figure 4a the mean cluster size is 28 ± 8 nm and in Figure 4b 70 ± 40 nm. Clusters corresponding to the diffraction patterns in Figures 1c and 1f were also deposited and studied by FE-SEM. The images reveal that the cluster beam comprises of a mixture of crystalline and spherical, amorphous particles. The amorphous particles

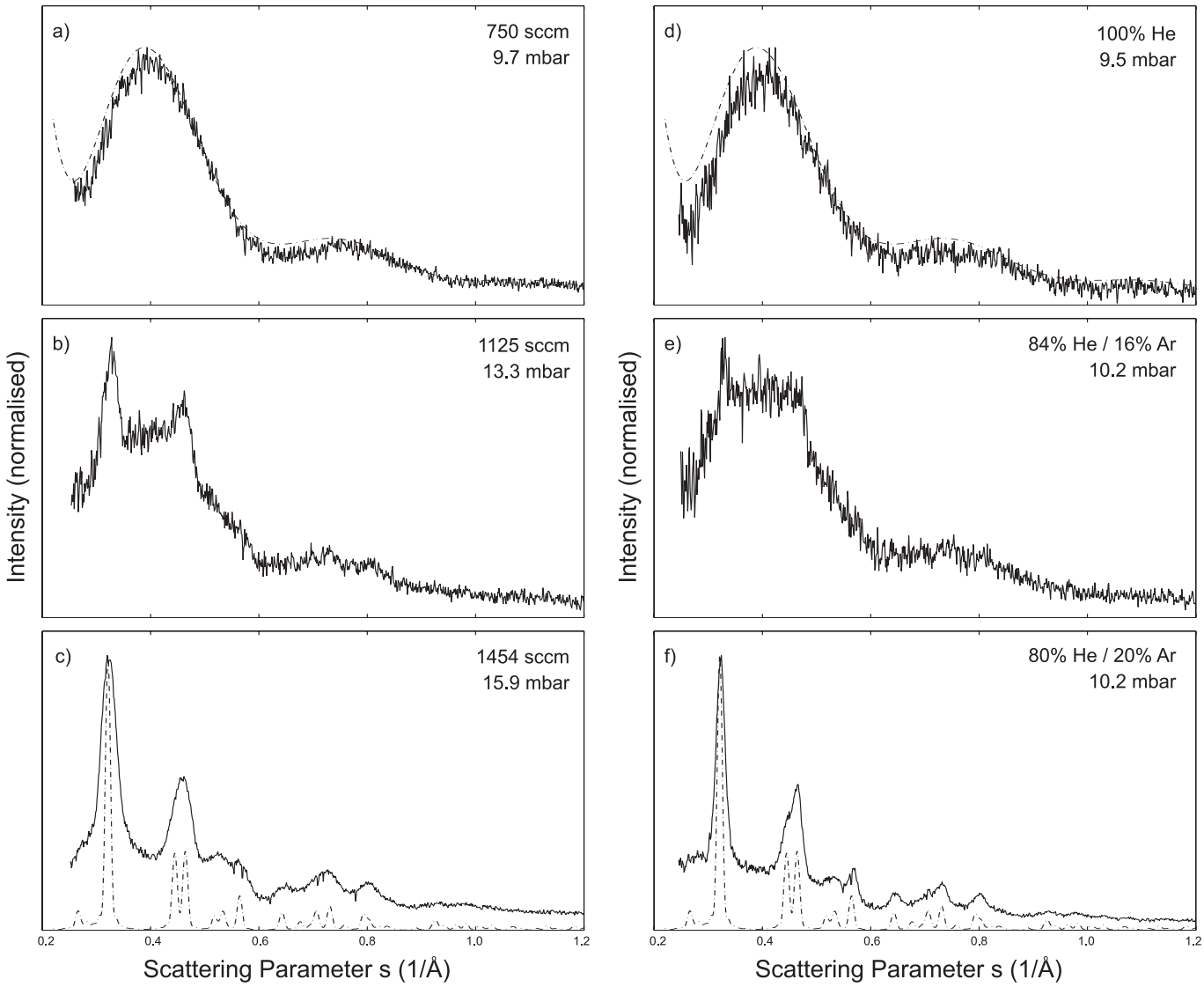

Fig. 2. Diffraction patterns of Sb clusters using helium and a helium/argon mixture as cooling gas. (a–c) The flow rate is increased while the temperature is kept constant at 700 °C. (d–f) The Ar content is increased while the total flow rate and the temperature is left constant (600 sccm and 700 °C respectively). The dotted lines in figures (a) and (d) show the calculated pattern for Sb_4 and in figures (c) and (f) the calculated pattern for a spherical cluster with rhombohedral structure and 10 nm diameter. Note: there is no additional offset applied to any of the patterns but the calculated patterns are scaled to match the height of the experimental patterns. The background visible in the experimental patterns in (c) and (f) might be due to Sb tetramers.

corresponding to the diffraction pattern in Figure 1c have a mean size of 35 ± 4 nm and the crystalline particles of 120 ± 40 nm. For Figure 1f the mean sizes are 30 ± 10 nm and 220 ± 150 nm respectively.

The size distribution for crystalline clusters in the SEM images is in obvious contradiction to the size estimates obtained from the diffraction patterns. There are three possible explanations: firstly, the clusters might be smaller in the beam but grow on the substrate through aggregation. This can be ruled out due to the morphology of the film (Figs. 4a and 4b); the loose packed 3D structure is consistent with the random deposition of large crystalline particles but inconsistent with diffusion and aggregation of smaller clusters [20]. Secondly, it is well established that diffraction patterns reflect the structure of domains rather than the whole cluster [21]. However, the presence of uncorrelated domains seems unlikely in the case of facetted, well defined crystallites such as those shown in Figure 4b. Thirdly, many FE-SEM images show that there is a mixture of crystalline and amorphous particles, even though the diffraction pattern shows strong crystalline features. As the peaks in the diffraction pattern from amorphous particles occur at similar scattering angles to the main peaks for crystalline particles, the resultant peak broadening most likely invalidates the use of the Scherrer equation and the comparison with calculated patterns.

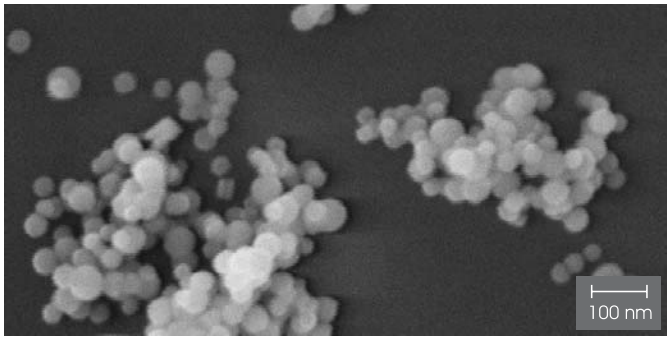

Fig. 3. An FE-SEM image of amorphous clusters as described in Section 3.1 and corresponding to the broad diffraction pattern in Figure 1d. The source conditions used were 675 °C and 82 sccm Ar (P_G = 4.8 mbar). Clusters corresponding to the diffraction pattern in Figure 1a look very similar.

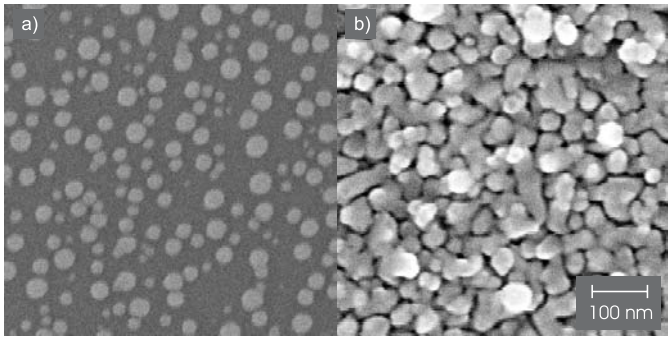

Fig. 5. Two FE-SEM image of Sb_4 clusters as described in Section 3.2. Both images are taken from the same sample. (a) Low coverage towards the edge of the cluster beam. (b) High coverage in the centre of the beam. The source conditions used were 700 °C, 520 sccm He, and 27 sccm Ar (P_G = 8.7 mbar).

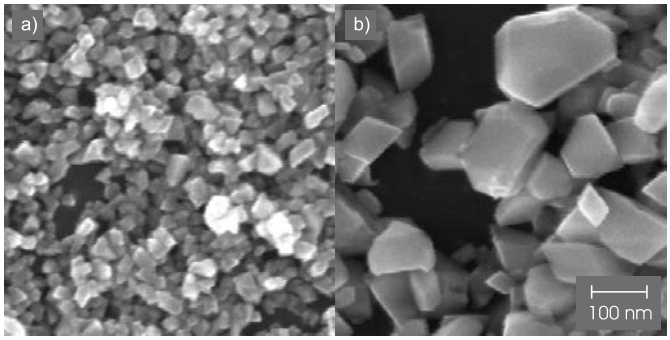

Fig. 4. Two FE-SEM images of clusters corresponding to the crystalline diffraction pattern as described in Sections 3.1 and 3.2. (a) The source conditions used were 700 °C, 120 sccm Ar, and 480 sccm He (P_G = 10.2 mbar) (corresponding to the diffraction pattern in Fig. 2f). (b) 750 °C and 158 sccm Ar (P_G = 5.5 mbar).

FE-SEM images of clusters which give rise to the diffraction patterns similar to these of Sb_4 are shown in Figures 5a and 5b. The mean size of the clusters is 26 ± 10 nm for Figure 5a and 35 ± 9 nm for Figure 5b. The mean particle size estimate does not differ significantly when comparing low coverage (Fig. 5a) to high coverage areas (Fig. 5b). In Figure 5a there are individual, well separated particles visible and in Figure 5b there are what appear to be individual clusters sitting in a second layer above a dense interconnected lower layer of clusters. This is not consistent with the deposition of Sb_4 tetramers. It appears, therefore, that the ∼30 nm particles in the beam consist of randomly oriented Sb_4 units. The lack of long-range order in such a particle and the absence of correlation between neighbouring Sb_4 units suggest that the diffraction pattern would be identical to that for isolated Sb_4 particles. This has been checked by calculation of diffraction patterns for 10 nm particles composed of randomly assembled Sb_4 units and indeed the diffraction patterns are identical to these of isolated Sb_4 tetramers.

It is noteworthy that the mean sizes for amorphous clusters and particles consisting of Sb_4 units are relatively uniform between 30 and 40 nm. The mean sizes for crystalline particles, however, vary hugely depending on the conditions.

4 Discussion and conclusions

Electron diffraction patterns have been obtained for Sb clusters with mean sizes of 30–40 nm and a range of different structures have been observed. Using Ar as cooling gas we observed a transition from an amorphous to a crystalline structure while increasing the source inlet gas flow rate or the temperature. FE-SEM images show that the amorphous particles are spherical, while the crystalline particles are strongly facetted. The size of the crystalline particles inferred from diffraction patterns is not consistent with the size distribution estimated from the FE-SEM images. The difference is most likely due to the presence of a mixture of crystalline and amorphous particles in the beam (observed on FE-SEM images) which makes simple analysis of the diffraction patterns inappropriate.

When He and a He/Ar mixture were used as the source inlet cooling gas, a transition from Sb_4 to crystalline diffraction patterns was observed for increasing flow rates or increasing Ar content. FE-SEM images suggest that individual Sb_4 units are not present in the beam but rather large clusters consisting of randomly oriented Sb_4 units. While structures composed of tetramers have been known to exist for a long time for As as well as P, an analogous structure for bulk Sb or Sb nanoparticles has never previously been observed.

Since no diffraction patterns were observed which correspond to the fcc structures proposed by Sattler, the packing of Sb_4 tetramers to form a compact crystalline structure can be ruled out in the present experiments. Instead, on the basis of the data reported here, it appears that Sattler's mass spectra [3] might be better explained using a model which incorporates a random (amorphous or liquid) packing of tetramers. It should be noted, however, that Sattler's experiments focussed on very small Sb

particles (up to Sb_{240}), while the clusters in our study had mean sizes of at least 20 nm.

References

1. A.F. Holleman, N. Wiberg, *Inorganic Chemistry* (Academic Press, San Diego, 2001)
2. T.M. Bernhardt et al., Angew. Chem. Int. Ed. **42**, 199 (2003)
3. K. Sattler et al., Phys. Lett. **87A**, 418 (1982)
4. G.D. Stein, *Metal cluster beams and electron diffraction: Deviations from the bulk state of matter*, unpublished, 1982
5. L. Sun et al., Mater. Sci. Eng. A **217**, 15 (1996)
6. B.D. Hall et al., Rev. Sci. Instr. **62**, 1481 (1991)
7. D. Reinhard et al., Phys. Rev. B **55**, 7868 (1997)
8. D. Reinhard et al., Phys. Rev. Lett. **79**, 1459 (1997)
9. M. Hyslop et al., Eur. Phys. J. D **16**, 233 (2001)
10. A. Wurl et al., Eur. Phys. J. D **16**, 205 (2001)
11. J.G. Partridge et al., Nanotechnology **15**, 1382 (2004)
12. A. Guinier, *X-Ray Diffraction in Crystals, Imperfect Crystals, and Amorphous Bodies* (W.H. Freeman and Company, San Francisco and London, 1963)
13. R.W.G. Wyckoff, *Crystal Structures* (Interscience Publishers, New York, 1963), Vol. 1
14. V. Sundararajan, V. Kumar, J. Chem. Phys. **102**, 9631 (1995)
15. B.V. Reddy, P. Jena, Chem. Phys. Lett. **288**, 253 (1998)
16. X.-W. Zou, Z.-Z. Jin, S.-Q. Tang, Phys. Stat. Sol. (b) **142**, 9 (1987)
17. Diffraction patterns from fcc particles are shown in D. Reinhard et al., Phys. Rev. B **58**, 4917 (1998)
18. J.A. Prins, Nature **131**, 760 (1933)
19. H. Richter, H. Berckhemer, G. Breitling, Z. Naturforschg, **9A**, 236 (1954)
20. P. Melinon et al., Phys. Rev. B. **44**, 12562 (1991)
21. B.D. Hall, J. Appl. Phys. **87**, 1666 (2000)